

Molecular clouds as the origin of the Fermi gamma-ray GeV-excess

Iris Gebauer*, Wim de Boer, Leo Bosse, Alexander Neumann

Karlsruhe Institute of Technology, Institute for Experimental Nuclear Physics, D-76131

Karlsruhe, Germany

E-mail: gebauer@kit.edu

Peter L. Biermann

MPI for Radioastronomy, Bonn, Germany

Dept. of Phys., Karlsruhe Inst. for Technology KIT, Karlsruhe, Germany

Dept. of Phys. & Astr., Univ. of Alabama, Tuscaloosa, AL, USA

Dept. of Phys. & Astron., Univ. Bonn, Bonn, Germany

The Fermi-LAT data reveal an excess of diffuse gamma-rays at energies of around 2 GeV in the direction of the Galactic center. The excess has been studied by many groups and is observed above the expectation for diffuse gamma-ray emission from cosmic ray interactions with the interstellar material (π^0 production from cosmic ray protons and bremsstrahlung from electrons in the interstellar gas) and the interstellar radiation field (inverse Compton scattering of electrons in the interstellar radiation field). In addition to these standard components in diffuse gamma-rays we find evidence for two additional processes: π^0 production in sources during acceleration and π^0 production in molecular clouds.

The first one is characterized by nuclear cosmic rays with a hard E^{-2} spectrum, expected from diffusive shockwave acceleration and can be traced by the 1.8 MeV gamma-ray line from radioactive ^{26}Al decays, which is synthesized in sources. The second one is characterized by nuclear cosmic rays inside molecular clouds with a sharp cutoff below 6-14 GV, which is most clearly observed in the dense Central Molecular Zone encircling the Galactic center in the Galactic disk. The cutoff leads to a suppression of low energy cosmic ray interactions in molecular clouds, which causes a shift in the maximum of the gamma-ray spectrum to higher energies, the hall-mark of the GeV-excess. This was previously interpreted as a dark matter annihilation signal.

No spatial information is provided to our fit. As a result we obtain an uncorrelated and spatially highly resolved distribution of the GeV-excess. We show that a shift in the maximum of the gamma-ray spectrum, or equivalently the GeV-excess, is observed in all directions, where molecular clouds are present; these directions are available from the high resolution all-sky CO maps from the Planck satellite.

35th International Cosmic Ray Conference — ICRC2017

10–20 July, 2017

Bexco, Busan, Korea

*Speaker.

1. Introduction

An apparent excess of diffuse gamma-rays in the the Fermi-LAT data around energies of 2 GeV towards the Galactic center has been studied by many groups. The GeV-excess is usually assumed to originate from the Galactic center with the most exciting interpretations being the contributions from dark matter (DM) annihilation [1] and/or unresolved sources, like millisecond pulsars, see e.g. Refs. [2, 3] and references therein.

The conventional approach to search for excesses is the use of *spatial* templates for the gas and interstellar radiation field, which are the targets for the background processes: π^0 production by propagated cosmic rays (PCR), Bremsstrahlung (BR) and inverse Compton (IC) scattering.

For the spatial templates of the above backgrounds one either uses the emissivity of propagation models, as studied e.g. in Ref. [4] or one uses a diffuse model from Fermi as spatial template, as done e.g. in Ref. [1]. Neither one provides a good description of the inner Galaxy and the Galactic disk, since the fitting of spatial templates implies fitting over extended regions, thus averaging over rapidly varying emissivities, like the emissivity from molecular clouds (MCs) or unresolved sources.

Here we follow an approach orthogonal to the approaches described above: instead of *spatial* templates we use *spectral* templates, one for each physical process describing the gamma-ray spectrum for that specific process. This ansatz allows to identify whether additional spectral templates are required. We find that the data require two additional components on top of the PCR, BR and IC components: (i) cosmic rays inside MCs (MCRs) which lead to a shift of the maximum of the gamma-ray spectrum from 0.7 GeV to up to 2 GeV, as is apparent from the spectrum of the Central Molecular Zone. The mass of the CMZ accounts for about 5% of the total molecular mass of the Milky Way, which means that towards the CMZ the gamma-ray emission is expected to be dominated by interactions in MCs. The origin of the shift in the maximum of the emissivity of MCs is possibly caused by a magnetic cutoff of cosmic rays approaching MCs. Such a cutoff is observed for cosmic rays entering the Earth's magnetic field: particles below typically 20 GV entering near the magnetic equator do not reach the Earth, but are deflected into outer space [5]. Variations in the magnetic cutoff in MCs are expected from the variations in size and in magnetic field which varies with the square of the density [6]. We find that variations of the break in the proton spectrum between 14 and 6 GV describe the gamma-ray data. (ii) Cosmic rays inside unresolved sources (SCRs) lead to a hard spectrum by the π^0 production in the shocked gas, as was first discussed in detail in Ref. [7], which leads to a high energy tail in the gamma-ray emissivity. This tail was investigated in Refs. [8, 9] and its correlation with unresolved sources is apparent from the spatial correlation with the 1.8 MeV line from ^{26}Al , which traces sources. [10].

2. Analysis

The data selection is described in [11, 8, 9]. The sky maps are rebinned to form a total of 797 cones covering the whole sky. In and around the Galactic disk the cones are one degree in latitude with a longitude size adapted to the structures, like the CMZ and the Fermi Bubbles. In the halo the cone size increases in regions without structure, i.e. outside the Fermi Bubbles, typically to

18.5°(10°) for latitudes above 55°(5°), while the cone size in longitude was increased similarly. The precise cone sizes and fit results for each of the 797 cones are given in [11].

The total flux in a given direction can be described by a linear combination of the gamma-ray fluxes from various processes:

$$|\Phi_{tot} \rangle = n_1 |\Phi_{PCR} \rangle + n_2 |\Phi_{BR} \rangle + n_3 |\Phi_{IC} \rangle + n_4 |\Phi_{SCR} \rangle + n_5 |\Phi_{MCR} \rangle + |\Phi_{ISO} \rangle, \quad (2.1)$$

where the normalization factors n_i determine the fraction of the total flux for a given process. $|\Phi_{ISO} \rangle$ is the isotropic background. The factors n_i can be found from a χ^2 fit, which adjusts the intensity n_i of the gamma-ray fluxes from the spectral templates to best describe the data. Including the spectral knowledge of all processes leads to an over-constrained fit for each field-of-view in a certain sky direction (called cones in the following), since the observed gamma-ray spectrum for a certain cone has 21 data points (= 21 energy bins) with only $n_i \leq 6$ free parameters. As a result one obtains an uncorrelated and spatially highly resolved distribution of the GeV-excess.

As test statistic we use the χ^2 function defined as

$$\chi^2 = \sum_{i=1}^N \sum_{j=1}^{21} \left[\frac{(\langle data(i, j) - \sum_{k=1}^5 n(i, k) \times tem(i, j, k) - |\Phi_{ISO} \rangle)^2}{\sigma(i, j)^2} \right], \quad (2.2)$$

where the sum is taken over the $N=797$ cones in different sky directions i , $data(i, j)$ represents the total Fermi-LAT gamma-ray flux in direction i for energy bin j , $tem(i, j, k)$ the template contribution with normalization $n(i, k)$ for template k and $\sigma(i, j)$ is the total error on $data(i, j)$, obtained by adding the statistical and systematic errors in quadrature. Details on the fit and the treatment of the Fermi systematic errors can be found in [11].

2.1 Determination of spectral templates

The spectral templates for the various processes in Eq. 2.1 are obtained from the gamma-ray data and local cosmic ray measurements. We assume that the leptons and nuclei follow a power law spectrum in the interstellar space with at most one break. The gamma-ray templates are determined in an iterative way: as a first estimate the spectral index of the locally observed cosmic rays above 20 GV, a region which is not influenced strongly by solar modulation is used. We then perform a fit to the gamma-ray data, modify the cosmic ray spectra and fit again. This procedure is iterated until the best fit to the gamma-ray data is obtained. In this way the templates are obtained for all processes without the need for a propagation model. The resulting templates and corresponding cosmic ray power law spectra are shown in Fig. 1. In addition, an isotropic template represents the contribution from the isotropic extragalactic background and hadron misidentification. The isotropic template was determined from the data, details can be found in [11].

Details on the PCR and SCR templates The proton spectra for the PCR and SCR templates can be described by an unbroken power law ($R^{-\alpha}$) with a spectral index (α) of 2.85 and 2.1, respectively, as obtained from the best fit. The index 2.85 corresponds to the index from the AMS-02 proton data [12]. The index 2.1 for the SCR template agrees with the data from the Fermi Bubble and is expected from diffuse shock wave acceleration [13, 14].

Details on the MCR template We parametrize the decreasing gamma-ray emissivity from MCs below the magnetic cutoff by a break in the power law of the corresponding proton spectrum. Above the break the the MCR template is identical to the PCR template, but below the break, which varies according to the fit from 6 to 14 GV for the different clouds, a spectral index of 0.7 was found, thus providing a significant suppression of protons below the break.

Details on the BR and IC templates The interstellar electron spectra require a break around 1 GeV with a spectral index of 3.21 above the break compatible with the locally observed electron spectrum (see Fig. 1(b)) and a spectral index of 0.81 below the break of 1 GeV, which implies a suppression of electrons. The break might be related to the minimum of the electron energy losses, since above this energy synchrotron and IC dominate the energy losses, while below this energy ionization losses become strong, thus depleting the electron spectrum below 1 GeV. Since the photon composition of the ISRF varies with sky direction, the IC templates have to be calculated for each sky direction. The variation over the sky is about $\pm 10\%$, as shown in [11].

Details on the DM template DM particles are expected to annihilate and the annihilation energy of roughly twice the WIMP mass will lead to the production of hadrons, thus producing copiously gamma-rays from π^0 decays. The annihilation signal peaking at 2-3 GeV requires a WIMP mass around 44.9 GeV, as shown in Fig. 1(a) as well. The difference to the MCR template is the cutoff at twice the WIMP mass, which is absent in the MCR template.

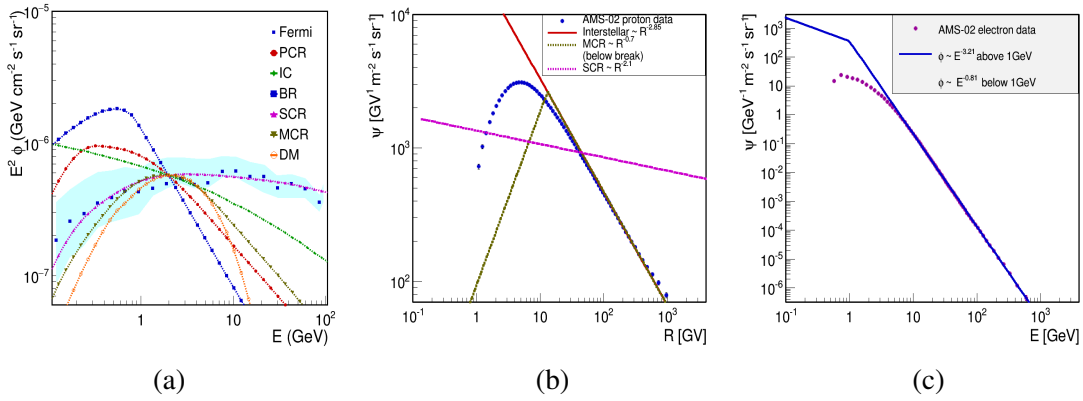


Figure 1: (a) Diffuse gamma-ray spectral templates for Bremsstrahlung (BR), inverse Compton scattering (IC) and π^0 productions by propagated cosmic rays (PCRs), cosmic rays inside unresolved point sources (SCRs) and cosmic rays inside MCs (MCRs). The templates are normalized around 2 GeV. The blue band shows the allowed region for the gamma-ray spectra from the Fermi Bubbles [15], which is consistent with the SCR template. Also shown is the gamma-ray template expected for a DM candidate with a mass of 44.9 GeV annihilating into $b\bar{b}$ quark pairs. (b) Power law proton cosmic ray spectra describing the PCR, MCR, and SCR gamma-ray templates in (a). (c) A power law electron cosmic ray spectrum with a break at 1 GeV describing the IC and BR gamma-ray templates in (a). At high energies the power law cosmic ray spectra have spectral indices compatible with the ones from the locally observed electron and proton data from AMS-02 [16, 12], which are shown as well. The spectra are normalized at 70 GV.

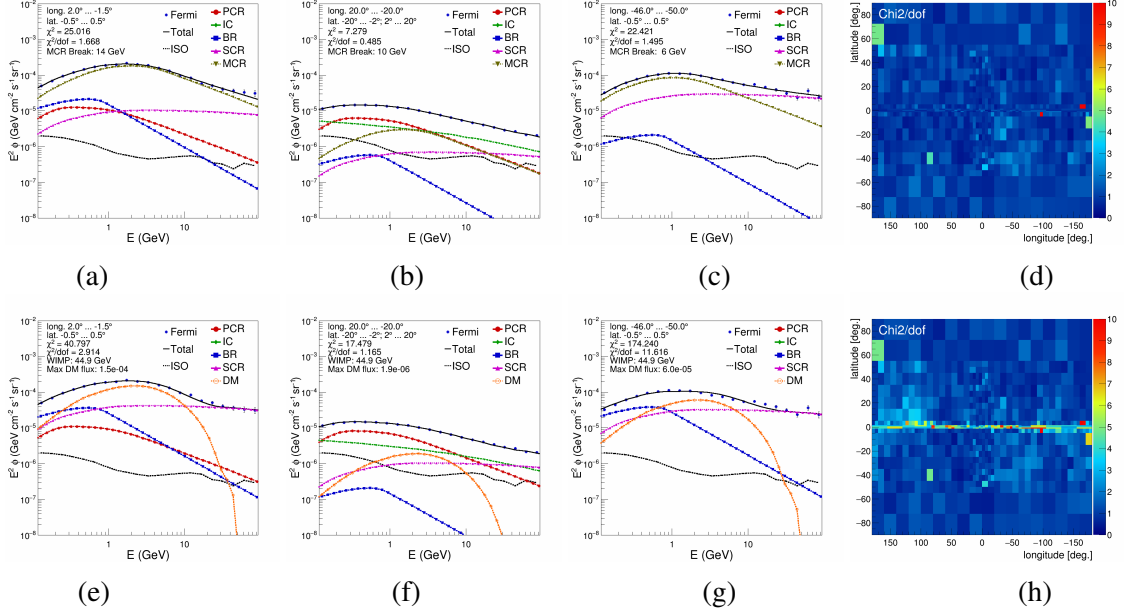


Figure 2: Spectral template fits to the Fermi diffuse gamma-ray data for the following regions of interest: towards the CMZ (first column), halo (middle column) and the nearby tangent point of the Scutum-Centaurus arm (last column) using either the MCR template (top) or DM template (bottom). The last column shows the χ^2/dof values of fits in all 797 cones with either the MCR template (top) or the DM template (bottom).

3. Results

The fit is performed using all physical templates described above. In a first fit the MCR template is used to account for the GeV excess, in a second fit the DM template is used. For the MCR template the fit is allowed to try all MCR break positions between 6 and 14. The fit is supposed to find out if the expected backgrounds from the PCR, BR, IC and ISO templates fit the data or if the maximum of the spectrum is shifted (a feature recognized by the DM or MCR template) or if the data has a high energy tail above the expectations from the known backgrounds (a feature recognized by the SCR template).

Fits in three cones are shown as examples in Fig. 2: one for the Galactic center, where the size of the CMZ has been selected ($-1.5^\circ < l < 2^\circ$ and $|b| < 0.5^\circ$), one in the halo with $-20^\circ < l < 20^\circ$ and $2^\circ < |b| < 20^\circ$ and one along the nearby tangent point of the Scutum-Centaurus spiral arm with $-50^\circ < l < -46^\circ$ and $-0.5^\circ < |b| < 0.5^\circ$. The top(bottom) panels show the fits with the MCR(DM) template. The best fitted break in the proton spectrum for the MCR template is indicated in the fits on the top, while the maximum of the DM flux is indicated for the DM fits on the bottom. The DM fits all use a WIMP mass of 44.9 GeV, which is the optimal mass for the Galactic center. Both, the WIMP mass and the DM flux from our analysis with energy templates are compatible with other analyses. [1, 18]

We checked that the GeV-excess is maximal inside the rectangular field-of-view of the CMZ by repeating the fit with a sliding window of constant size. The fact that the GeV-excess has a longitudinally elongated morphology in the inner few degrees of the Galactic center strongly disfavors the DM interpretation.

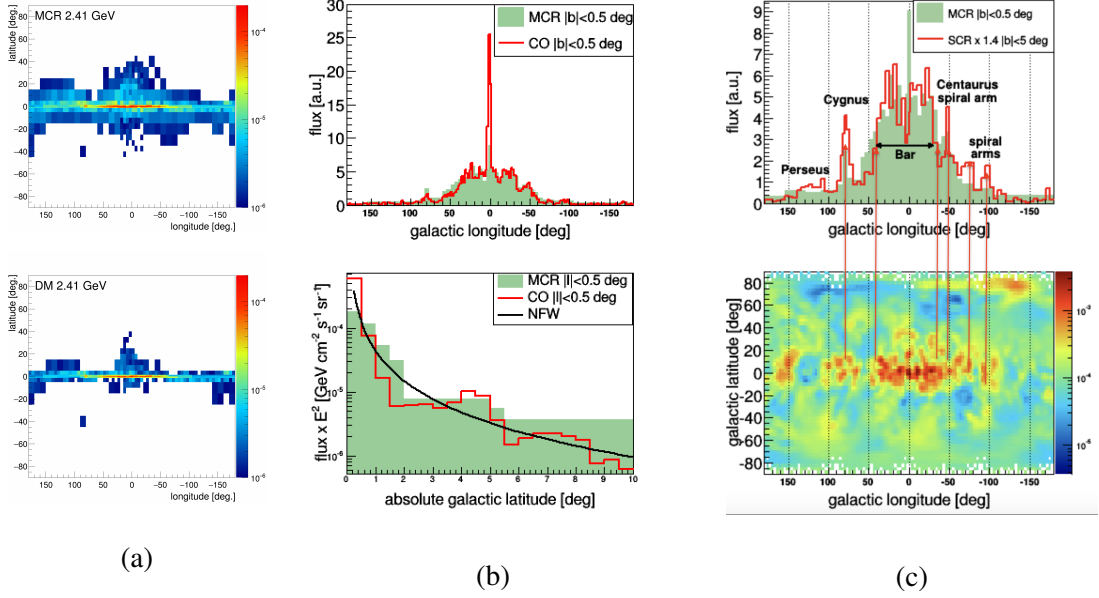


Figure 3: (a) Sky maps of the fluxes of the MCR template (top) for a DM candidate with a mass of 44.9 GeV annihilating into $b\bar{b}$ quark pairs (bottom). The fluxes are in units of $\text{GeV cm}^{-1} \text{s}^{-1} \text{sr}^{-1}$ at an energy of 2.41 GeV. (b) Longitude and latitude profile of the MCR template (green histogram, this analysis) and CO (red line) [17]. The fluxes from MCR and CO sky maps are normalized. The black line in the bottom panel corresponds to the NFW template from Fig. 1 from Ref. [18]. One observes that the CO latitude distribution from the Planck satellite resembles an average NFW profile with some clumpiness. (c) the longitude distribution of the fluxes from the SCR and MCR templates, which have a similar morphology, since both are connected to MCs. The gamma-ray fluxes from the SCR (MCR) templates are integrated over a latitude range of $|b| < 6^\circ$ (0.5°), respectively. The larger latitude range for the SCR component pays tribute to the fact that the sources have outflows towards higher latitudes. The lower panel shows the ^{26}Al sky map [19, 20] in units of $\text{cm}^{-2} \text{s}^{-1} \text{sr}^{-1}$, which is correlated with the top panel, as indicated by the vertical arrows. This correlation is expected, since both, the ^{26}Al flux and the SCR flux, are tracers of cosmic ray sources.

One observes better fits with the MCR template, as can be seen from the reduced χ^2 values in Fig. 2. The MCR fits also reveal the expected BR contribution, which is absent with the DM template fit, since here the long tail in the data is not described by the DM template with its decreasing contribution above 10 GeV. Note that the spatial template analyses usually do not distinguish between Bremsstrahlung and gamma-rays from π^0 production, since these contributions are both proportional to the same gas template.

The SCR template in the middle column has the contributions from both, the π^0 production inside point sources and in the Fermi Bubble, since they both contribute in this field-of-view up to latitudes of 20° , but have the same hard SCR template. Note that our analysis does not need the spatial template for the Fermi Bubble, since its contribution is determined by the energy template for each cone.

The third column in Fig. 2 shows the fits towards the tangent point of the Scutum-Centaurus arm. Here the data are again dominated by the GeV-excess, which is not expected for a DM halo.

The fits to all 797 cones are shown in the Appendices of [11], both for the MCR and DM template fits.

No spatial information is provided to the fit. Consequently, the sky maps of the various contributions can be directly obtained by plotting the fitted normalization constants in Eq. 2.1. The sky map of the GeV-excess corresponds to the sky maps of either the MCR or DM template, which are shown in Fig. 3a. One observes in both cases a strong component along the disk with rapidly decreasing latitude contributions up to $15\text{-}20^\circ$. A comparison between the MCR sky map and the CO sky map is shown in Fig. 3b. Both show a strong contribution from the CMZ and the bar. The longitude distribution decreases rapidly outside the Galactic Bar region. The latitude distribution resembles for both fluxes the flux expected from a DM annihilation signal proportional to the expectation from a generalized NFW profile, which was taken from Fig. 1 in Ref. [18].

A correlation between the SCR and MCR fluxes is observed, as shown in the top panel of Fig. 3c. This is expected since sources are expected to reside inside MCs. The bottom panel of Fig. 3c shows a map of the 1.8 MeV ^{26}Al line emission as observed by Integral/SPI[19]. The radioactive ^{26}Al isotope is synthesized by proton capture of ^{25}Mg in heavy, magnesium rich sources [10] and can be traced by the 1.8 MeV gamma-line emitted in its decay. The correlation between the SCR fluxes, MCR fluxes and ^{26}Al fluxes is emphasized by the vertical arrows in Fig. 3(b) between the sky map of the ^{26}Al line (bottom panel) and the longitude distribution of the SCR and MCR fluxes (top panel).

4. Conclusion

We have compared two hypothesis for the GeV-excess: an excess of gamma-rays peaking around 2 GeV from DM annihilation (DM hypothesis) or a depletion of gamma-rays below 2 GeV as observed in the gamma-ray emissivity of MCs (MC hypothesis). We find that the MC hypothesis is preferred over the DM hypothesis for the following reasons: i) the MC hypothesis provides a significantly better fit, especially if one considers the gamma-ray energies up to 100 GeV. ii) the GeV-excess has for both hypotheses the morphology expected from a generalized NFW profile in latitude (see bottom panel of Fig. 3(a) for the MCR template), but shows in longitude a strong flux towards MC regions in the Galactic disk. In particular, the DM sky map does not resemble the expected spherical DM halo profile, but has a morphology similar to the CO sky map, as demonstrated in Fig. 3(a).

References

- [1] T. Daylan, D. P. Finkbeiner, D. Hooper, T. Linden, S. K. N. Portillo, N. L. Rodd, and T. R. Slatyer, “The characterization of the gamma-ray signal from the central Milky Way: A case for annihilating dark matter,” *Phys. Dark Univ.*, vol. 12, pp. 1–23, 2016.
- [2] R. Bartels, S. Krishnamurthy, and C. Weniger, “Strong support for the millisecond pulsar origin of the Galactic center GeV excess,” *Phys. Rev. Lett.*, vol. 116, no. 5, p. 051102, 2016.
- [3] D. Hooper and G. Mohlabeng, “The Gamma-Ray Luminosity Function of Millisecond Pulsars and Implications for the GeV Excess,” *JCAP*, vol. 1603, no. 03, p. 049, 2016.
- [4] F. Calore, I. Cholis, and C. Weniger, “Background Model Systematics for the Fermi GeV Excess,” *JCAP*, vol. 1503, p. 038, 2015.

- [5] Herbst, K., Kopp, A. and Heber, B., “Influence of the terrestrial magnetic field geometry on the cutoff rigidity of cosmic ray particles,” *Ann. Geophys.*, vol. 31, pp. 1637–1643, 2013.
- [6] R. M. Crutcher, “Magnetic Fields in Molecular Clouds,” *Annual Rev. of Astrop.*, vol. 50, no. 1, pp. 29–63, 2012.
- [7] E. G. Berezhko and H. J. Volk, “Galactic gamma-ray background radiation from supernova remnants,” *Astrophys. J.*, vol. 540, pp. 923–929, 2000.
- [8] W. de Boer and M. Weber, “Fermi Bubbles and Bubble-like emission from the Galactic Plane,” *Astrophys. J.*, vol. 794, no. 1, p. L17, 2014.
- [9] W. De Boer, “Evidence for a hadronic origin of the Fermi Bubbles and the Galactic Excess,” *PoS*, vol. ICRC2015, p. 907, 2016.
- [10] Prantzos, N. and Diehl, R., “Radioactive ^{26}Al in the Galaxy: Observations versus Theory,” *Phys. Rep.*, vol. 267, pp. 1–96, 1996.
- [11] W. de Boer, L. Bosse, I. Gebauer, A. Neumann, and P. Biermann, “Molecular Clouds as the Origin of the Fermi Gamma-Ray GeV-Excess,” *accepted for publication in Phys. Rev. D*, July 2017.
- [12] M. Aguilar *et al.*, “Precision Measurement of the Proton Flux in Primary Cosmic Rays from Rigidity 1 GV to 1.8 TV with the Alpha Magnetic Spectrometer on the International Space Station,” *Phys. Rev. Lett.*, vol. 114, p. 171103, 2015.
- [13] A. Hillas, “Can diffusive shock acceleration in supernova remnants account for high-energy galactic cosmic rays?,” *J.Phys.*, vol. G31, pp. R95–R131, 2005.
- [14] P. L. Biermann, J. K. Becker, J. Dreyer, A. Meli, E.-S. Seo, *et al.*, “The origin of cosmic rays: Explosions of massive stars with magnetic winds and their supernova mechanism,” *Astrophys.J.*, vol. 725, pp. 184–187, 2010.
- [15] M. Ackermann *et al.*, “The Spectrum and Morphology of the Fermi Bubbles,” *Astrophys. J.*, vol. 793, no. 1, p. 64, 2014.
- [16] M. Aguilar *et al.*, “Electron and Positron Fluxes in Primary Cosmic Rays Measured with the Alpha Magnetic Spectrometer on the International Space Station,” *Phys. Rev. Lett.*, vol. 113, p. 121102, 2014.
- [17] , The fits file COM_CompMap_CO21-commander_2048_R2.00.fits was downloaded from: https://wiki.cosmos.esa.int/planckpla2015/index.php/CMB_and_astrophysical_component_maps#CO_line_emission/, 2015.
- [18] F. Calore, I. Cholis, C. McCabe, and C. Weniger, “A Tale of Tails: Dark Matter Interpretations of the Fermi GeV Excess in Light of Background Model Systematics,” *Phys. Rev.*, vol. D91, no. 6, p. 063003, 2015.
- [19] L. Bouchet, E. Jourdain, and J.-P. Roques, “The Galactic ^{26}Al emission map as revealed by INTEGRAL/SPI,” *Astrophys. J.*, vol. 801, no. 2, p. 142, 2015.
- [20] Integral-SPI The data was downloaded from: <http://sigma-2.cesr.fr/integral/aluminium-map&source>, 2015.